chemistry

MDPI

Article

Facile Synthesis of Zeolite NaX from Natural Attapulgite Clay for Pb^{2+} Adsorption

Min Feng [1], Zhiming Shi [1], Yongchun Tong [1,*] and Kewei Zhang [2,*]

[1] Key Laboratory of Hexi Corridor Resources Utilization of Gansu, College of Chemistry and Chemical Engineering, Hexi University, Zhangye 734000, China; hxxyfm@126.com (M.F.)
[2] College of Materials Science and Engineering, Qingdao University, Qingdao 266071, China
* Correspondence: tongjia12@163.com (Y.T.); zhkw@qdu.edu.cn (K.Z.)

Abstract: The synthesis of zeolites from natural aluminosilicate minerals has drawn extensive attention due to its significant utility in greening the zeolite manufacturing process. In this study, pure-phase NaX zeolite was synthesized via a low-temperature hydrothermal method, utilizing natural, low-quality attapulgite clay as the raw material. Acidified clay was fully activated through alkali fusion at 200 °C, and the impact of alkali fusion temperature, H_2O/Na_2O ratio, aging temperature, and crystallization time on the resulting crystalline NaX zeolite was investigated. The optimal conditions for obtaining pure NaX zeolite were determined to be alkali melting at 200 °C for 4 h, an H_2O/Na_2O ratio of 50, aging at 40 °C, and a crystallization period of 11 h at 90 °C. With a large BET surface area of 328.43 m^2/g, the obtained NaX zeolite was used to adsorb Pb^{2+} from wastewater with a removal rate of 95%. This research provides a valuable method for the extensive and efficient utilization of low-grade natural attapulgite clay. Moreover, this is the first report on the synthesis of pure-phase NaX zeolite using only low-quality natural attapulgite clay as raw material through an atmospheric pressure water bath method.

Keywords: NaX zeolite; attapulgite clay; water bath; Pb^{2+}

Citation: Feng, M.; Shi, Z.; Tong, Y.; Zhang, K. Facile Synthesis of Zeolite NaX **from** Natural Attapulgite Clay for Pb^{2+} Adsorption. *Chemistry* **2024**, *6*, 1217–1229. https://doi.org/10.3390/chemistry6050070

Academic Editor: Matthias Lehmann

Received: 5 September 2024
Revised: 3 October 2024
Accepted: 9 October 2024
Published: 11 October 2024

1. Introduction

With the development of modern economy and industrial technology, heavy metal pollution has become a major environmental concern. Combating the pollution of heavy metals has become a hotspot of concern. Among them, Pb^{2+} is a common heavy metal pollutant, mainly from smelting, electroplating, storage batteries, paints and pigments, and other industries that produce wastewater. It is extremely important to prevent it from entering the human body and causing more harm after enrichment through the food chain [1,2]. Methods for treating lead-containing wastewater include chemical precipitation, ion exchange, electrolysis, membrane separation, etc., but all of them have the disadvantage of high treatment costs and complex processes. The adsorption method has been widely used due to its simple process, reusable adsorbent materials, and fast adsorption rate [3]. It is of great practical significance to develop low-cost and efficient adsorbents. Common adsorption materials for Pb^{2+} include activated carbon, ion exchange resins, biosorbents, metal–organic framework materials, and molecular sieves. Among these, molecular sieves have the advantages of higher selectivity, stronger renewability, lower cost, larger adsorption capacity, being easy to operate and manage, and being convenient for large-scale application. Therefore, it has broad application prospects in the field of wastewater treatment through the synergistic effect of molecular sieve effect and ion exchange effect.

Zeolite X has a unique three-dimensional pore structure, large specific surface area, and pore size [4,5], making it widely used in fields such as gas separation [6], water treatment [7], carbon dioxide capture [8], and catalyst industry [9]. At present, zeolite X is

mainly synthesized by the hydrothermal method with caustic soda, aluminum hydroxide, and water glass as raw materials, which has high production costs and pollution. Natural clay material has become an alternative material for zeolite synthesis due to abundant reserves, good performance, low cost, and no pollution. Kaolinite [10–13], illite [14–17], bentonite [18–20], diatomite [21–24], and coal fly ash [25–28] have been used for synthesizing zeolites, achieving a certain degree of green sourcing of raw materials and a reduction in the cost of raw materials.

Attapulgite clay minerals (ATP) are kinds of natural nanoscale water-rich magnesium-aluminum silicates with large reserves, low cost, and abundant pore channels, which are hot spots in the development and utilization of silicate minerals [29–31]. China has abundant and inexpensive ATP reserves, with more than 1 billion tons of clay reserves in Gansu Province alone, accounting for more than 74% of the world's proven reserves. The clays in this region are derived from clastic clay minerals in a lake environment with a high impurity content and low grade, making it difficult to achieve high value-added utilization [32–34]. Therefore, the development and utilization of low-grade clay have become a difficult problem for researchers.

In this work, we report the synthesis of pure-phase NaX zeolite by a simple low-temperature hydrothermal method using alkali fusion-activated low-grade natural attapulgite clay as raw material. The effects of H_2O/Na_2O ratio, crystallization time, aging temperature, and crystallization temperature on the crystalline products were systematically investigated. The crystal structure, surface morphology, pore structure, and surface properties of the synthesized products were characterized by XRD, SEM, BET, and FTIR. The clay-based NaX zeolite obtained then was used to treat Pb^{2+}-containing wastewater, and the effects of pH, initial concentration, adsorbent dosage, and effect of contact time on the removal rate of Pb^{2+} were investigated.

2. Experimental

2.1. Pretreatment Process of Natural Attapulgite Clay

The attapulgite clay utilized in this study was sourced from Zhengbei Mountain, Linze, China. The clay was crushed and then sieved through a 100-mesh sieve. The obtained sample was purified with the dispersant sodium hexametaphosphate to remove most of the quartz impurities. The sample was later acid-activated using hydrochloric acid of 4 mol/L to remove additional impurity components such as calcite from the clay. Analytically pure hydrochloric acid, sodium hydroxide, and sodium hexametaphosphate were procured from Sinopharm Reagent Co, Shanghai, China. Deionized water was prepared in-house.

2.2. Synthesis of NaX Zeolite

NaX zeolite samples were synthesized via a hydrothermal method following the alkali melting of pretreated natural attapulgite clay, which was used as a source of silica and alumina. To prepare the zeolite, sodium hydroxide was mixed with pretreated attapulgite clay at a 2:1 mass ratio, and the resulting mixture was ground and calcined in a ceramic crucible at 200 °C for 4 h. The fused mixture was subsequently cooled to room temperature and ground again. The resulting attapulgite clay mixture was mixed with deionized water at a ratio of 2:15 (2 g fused/15 mL water) and then aged with high-speed stirring (800 r/min) at 50 °C for 2 h. The mixture was then subjected to crystallization at 90 °C with low speed (300 r/min) for 8 h. The solids were separated via low-speed centrifugation, washed with deionized water until the pH approached 8, and subsequently dried and ground at 70 °C.

2.3. Heavy Metal Adsorption Experiment

In adsorption experiments, key factors affecting the adsorption effect were studied, including adsorption time, initial Pb^{2+} concentration, molecular sieve dosage, and pH value. Firstly, 0.09 g of NaX zeolite was added to 100 mL of simulated wastewater solution with a concentration of 100 mg/L. The samples were taken after 10, 20, 30, 60, 90, 120, 150, 180, 210, and 240 min of oscillatory adsorption at 25 °C. The supernatant was obtained by high-speed

centrifugation. After adding a color developer, the concentration of Pb^{2+} was determined by a UV spectrophotometer. Then the effect of molecular sieve dosage on Pb^{2+} removal was investigated. NaX zeolite of different masses (0.01 g, 0.03 g, 0.06 g, 0.09 g, 0.13 g, 0.16 g, and 0.19 g) were added to 100 mL of simulated wastewater solution with a concentration of 100 mg/L. Samples were taken for comparison after the adsorption was oscillated at 25 °C for 120 min. To study the effect of the initial concentration of simulated wastewater on the adsorption effect, 100 mL of each of the different solutions of C_0 (10 mg/L, 20 mg/L, 40 mg/L, 60 mg/L, 80 mg/L, 100 mg/L, 120 mg/L, and 140 mg/L) were taken, 0.09 g of NaX zeolite was added, and the adsorption was carried out by oscillation for 120 min under the condition of 25 °C. To study the effect of pH, the simulated wastewater was adjusted to pH 1–7 with 0.1 mol/L HNO_3 and 0.1 mol/L NaOH solutions, and 0.09 g of the prepared NaX zeolite was added to compare the removal effect after oscillatory adsorption. The removal rate η and the equilibrium adsorption capacity Q_e are calculated as follows:

$$\eta = \frac{C_0 - C_t}{C_0} \times 100\% \quad (1)$$

$$Q_e = \frac{V(C_0 - C_e)}{m_0} \times 100\% \quad (2)$$

where C_0 is the initial concentration of Pb^{2+} in the simulated wastewater (mg/L), C_t is the concentration of Pb^{2+} in the supernatant after adsorption (mg/L), and C_e is the concentration of Pb^{2+} in the supernatant when adsorption reaches equilibrium (mg/L). Q_e is the equilibrium adsorption capacity (mg/g), V is the volume of simulated wastewater (L); m_0 is the dosage of clay-based NaX molecular sieves (g).

2.4. Characterization

The chemical compositions of attapulgite clay were quantified using XRF (XRF-Axios, Panalytical, Almelo, The Netherlands). The crystal phase and mineral compositions of the samples were identified using X-ray diffraction (XRD-X'Pert3Powder Panalytical, Almelo, The Netherlands). Phase identification was conducted by leveraging the ICDD (Joint Committee on Powder Diffraction Standards) documentation for inorganic compounds. Fourier transform infrared spectroscopy (FT-IR) spectra were collected by a Nicolet iS50 spectrometer (Thermo Scientific, Waltham, MA, USA), with a spectral range of 400–4000 cm^{-1} and a resolution of 0.5 cm^{-1}, using the KBr technique. FE-SEM measurements were taken with a Quanta 450FEG scanning electron microscope (FEI, Brno, Czech Republic). The specific surface area and the pore diameter of the synthesized NaX were collected by the specific surface area and pore structure analyzer Tri StarII3020 (Micromeritics, Norcross, GA, USA).

3. Results and Discussion

3.1. Analysis of the Composition, Structure and Morphology of the Clay and the Obtained Zeolite NaX

According to Table 1, the natural attapulgite clay primarily comprises silica (43.9%), alumina (15.5%), sodium oxide (19.1%), and CaO (10.1%). Additionally, the clay contains several metallic Fe, Mg, and K elements and trace amounts of other elements. Figure 1 displays XRD patterns of raw attapulgite clay, acid-activated clay, and the alkali melted clay. The bottom curve in Figure 1 displays the X-ray diffraction pattern of the low-grade attapulgite clay. The diffraction peak at 8.544° (2θ value) corresponds to the diffraction peak of attapulgite clay. There are also two peaks at 26.718° and 29.505°, corresponding to the most prominent peak of quartz (SiO_2) and calcite ($CaCO_3$), respectively. These results suggest that the low-grade attapulgite clay in this region contains a substantial amount of crystalline quartz and calcite and attapulgite crystals. This finding is consistent with the compositional analysis results and aligns with the basic composition of the attapulgite clay in this region reported in the literature [33]. This low-quality mixed-dimensional attapulgite clay was subjected to alkali fusion activation to maximize the utilization of raw materials.

The upper two curves in Figure 1 present a comparison of the XRD patterns of the natural attapulgite clay before and after activation treatment. The purification and acidification resulted in the removal of some quartz and all calcite, while the typical characteristic peaks of the attapulgite clay were unaffected. After undergoing additional alkali fusion treatment, the main characteristic peaks and impurity peaks of the clay disappeared. It is believed that the quartz and amorphous materials reacted with NaOH during alkali fusion treatment, resulting in the formation of two new amorphous materials primarily comprised of sodium silicate ($NaSiO_3$) and sodium silicoaluminate ($NaAlSiO_4$). These materials serve as the primary active ingredients for zeolite synthesis. Therefore, acidification followed by alkali fusion treatment is an effective method for activating the natural attapulgite clay.

Table 1. Chemical composition (%) of the attapulgite clay sample determined by XRF.

Component	SiO_2	Al_2O_3	Fe_2O_3	CaO	MgO	K_2O	Na_2O
Content (wt%)	43.9	15.5	4.90	10.1	3.38	2.25	19.1

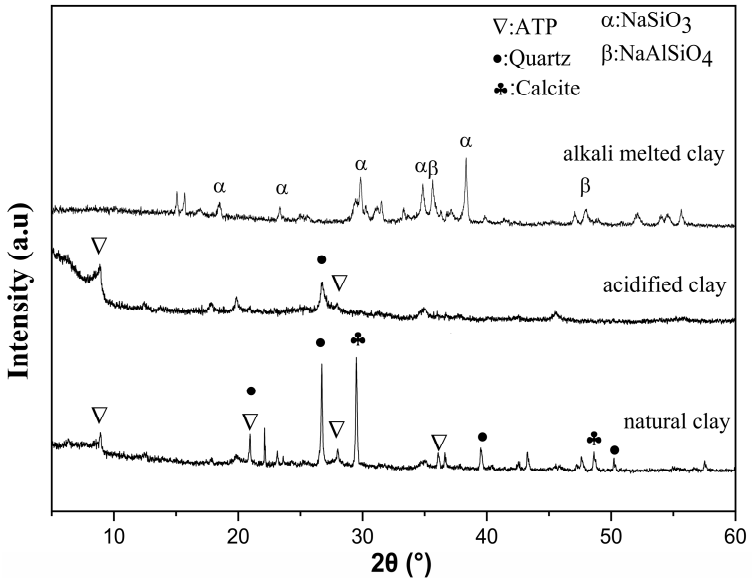

Figure 1. XRD patterns of the raw attapulgite clay, acid-activated clay, and the alkali-melted clay.

Figure 2a presents the SEM micrograph of the natural attapulgite clay, revealing not only short-rod attapulgite structures but also a significant accumulation of haphazardly arranged lamellar imonite. The particle size ranges from about 1 to 10 μm. The morphology of the synthesized NaX zeolites is depicted in Figure 2b,c. The particle is approximately 1.5 μm, exhibiting uniform particle size and good dispersion. The observed crystal structure exhibits an octahedral shape with a distinct and well-defined outline. The surfaces of the crystal are characterized by a substantial presence of adherent particles, indicating an adherent-type growth mechanism for zeolite in this specific system. This also indirectly proves the efficiency of the activation method used in the experiment. The alkali fusion process was able to fully activate the natural clay to sodium silicate and sodium silicoaluminate. The addition of water resulted in the formation of primary structural units required for zeolite synthesis, and these primary structures were reorganized and further condensed into polyhedral zeolite crystals [35]. Finally, the pure-phase NaX zeolite was obtained at the appropriate temperature, time, and alkalinity.

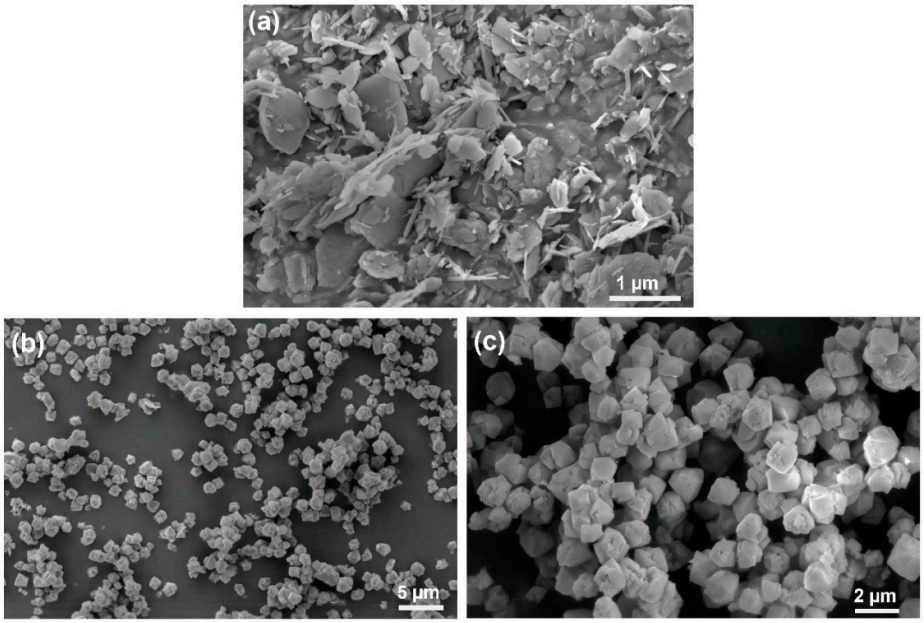

Figure 2. (**a**) SEM image of natural attapulgite clay. (**b**,**c**) SEM images of as-synthesized products under different magnifications.

The infrared spectroscopic analysis of NaX zeolite was performed, as shown in Figure 3a. Within the vibrational interval ranging from 4000 cm^{-1} to 400 cm^{-1}, seven prominent peaks associated with the framework vibrations of the zeolite were predominantly detected. The peaks at 984.79 cm^{-1} and 671.76 cm^{-1} are attributed to the symmetric stretching vibration and anti-symmetric absorption vibration of the silicon–oxygen tetrahedron and aluminum–oxygen tetrahedron, respectively. The peak observed at 460.44 cm^{-1} signifies the bending vibration of the T–O bonds within the zeolite. The notable intensities of these three absorption peaks indicate the existence of well-formed structural units of silicon–oxygen tetrahedra and aluminum–oxygen tetrahedra in the synthesized NaX zeolite. The characteristic peak observed at 562.61 cm^{-1} in the infrared spectrum confirms the presence of the D6R structure, comprising double six-membered rings, within the NaX zeolite. Moreover, a vibration peak at 749.48 cm^{-1} is attributed to the Si (Al)–O bonds. Additionally, the peaks at 3455.47 cm^{-1} and 1639.79 cm^{-1} correspond to the characteristic absorption of hydroxyl groups from the structural water and physically adsorbed water, respectively, in the NaX zeolite.

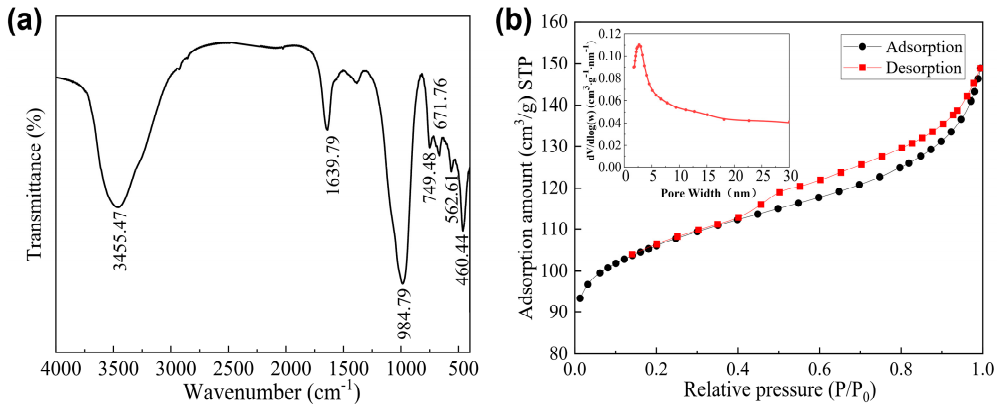

Figure 3. (**a**) FT-IR spectrum of as-synthesized NaX zeolite. (**b**) N_2 adsorption–desorption isotherm and pore size distribution of as-synthesized NaX zeolite.

To further investigate the structural characteristics of the sample and uncover the transformation of its specific surface area and pore structure, N_2 adsorption–desorption measurement was conducted. The sample was pretreated by drying at 250 °C under atmospheric pressure for 3 h. Subsequently, at an analysis bath temperature of −195.8 °C and with an equilibration interval of 30 s, 64 points were taken within the relative pressure (p/P_0) range from 0 to 1 for forward and reverse measurements. As shown in Figure 3b, the zeolite showed a typical type I isotherm but was not completely consistent, indicating that this material was primarily microporous and mesoporous. The N_2 adsorption–desorption curve of the synthetic zeolite exhibited a hysteresis loop within the pressure range of 0.4–1.0 p/P_0. This hysteresis loop lacks a distinct saturation adsorption platform and is classified as the H4 slit pore type among the four types of mesoporous hysteresis loops. This provides evidence that the pore channel structure of the prepared molecular sieve is intricate, consisting of a combination of micropores and mesopores, potentially including narrow slit pores. The obtained zeolite X showed a relatively high BET surface area of 328.43 $m^2\ g^{-1}$ with a micropore volume of 0.23 cm^3/g. The external surface area of 83.66 $m^2\ g^{-1}$ accounted for 25% of the BET surface area. The large external surface area and textural mesopores might have been the cause of the isotherm deviation from the type II isotherm. The external surface area and micropore volume were obtained by the t-plot method. The micropores exhibited a broad distribution of pore sizes, with the majority of pore sizes falling within the range of 3–5 nm.

3.2. Effect of Different Reaction Parameters on the Structure of Zeolite NaX

The commonly utilized activation methods for aluminosilicate clay minerals are high-temperature calcination activation and alkali fusion activation, both of which typically require a high-temperature environment exceeding 500–900 °C to achieve optimal results. In this experiment, the effects of different alkali fusion calcination temperatures (200 °C, 400 °C, and 600 °C) on the synthesized zeolites were investigated, as shown in Figure 4a. It can be seen that the samples synthesized with clays treated with alkali fusion at different temperatures all showed the typical diffraction peaks 2θ = 6.10, 9.97, 11.76, 15.39, 18.46, 20.12, 23.24, 26.58, and 30.86 of X zeolite (JCPDS 38-0237). These results confirm that the attapulgite clay activated at different temperatures can be utilized to synthesize highly crystalline and pure-phase X zeolite. The highest characteristic peaks of zeolites were especially synthesized after alkali fusion at 200 °C, which proved that the acidified clay could obtain a better activation effect at a relatively low temperature, providing high-quality active silicon and aluminum species for zeolite synthesis. This method significantly mitigates the energy consumption associated with raw material activation and provides an efficient and energy-saving treatment process for the pre-treatment of the clay. Subsequent experimental processes utilized 200 °C alkali fusion-activated clay as the primary raw material.

Water is essential in the hydrothermal synthesis of zeolites. On one hand, the constant synthesis conditions and the effect of H_2O/Na_2O on the synthesized zeolites were examined, and the results are illustrated in Figure 4b. With the increase in the H_2O/Na_2O ratio, the alkalinity of the system gradually decreased, and the crystallinity of the synthesized zeolite products demonstrated an initial rise followed by a decline. When the H_2O/Na_2O ratio reached 100:1, NaX zeolite was not obtained, and crystallographic phase analysis indicated that the primary product was a mixture of sodium silicate ($NaSiO_3$), sodium silicoaluminate ($NaAlSiO_4$), and amorphous material with very low crystallinity. This may be attributed to the low concentration of silica–alumina seeds in the precursors and the restricted alkalinity of the system. These factors hindered precursors and the restricted alkalinity of the system. These factors hindered zeolite nuclei formation and impeded the further growth of zeolite crystals. At a water/sodium ratio of 25:1, inadequate solvent leads to incomplete dissolution of silicon and aluminum seeds, resulting in insufficient crystal growth. Furthermore, excessively high alkali content under this condition leads to poor stability of zeolite in highly alkaline solutions and the generation of heterogeneous phases, which is unfavorable for zeolite synthesis. The optimal water/sodium ratio for synthesizing

NaX zeolite in this system is 50:1, which results in high crystallinity and a nearly pure phase. This ratio facilitates the dissolution of silicon and aluminum components in the precursor material, shortening the induction period and nucleation time and accelerating the crystallization rate, thereby promoting the synthesis of zeolite products. This phenomenon is attributed to the appropriate alkaline concentration and solvent amount.

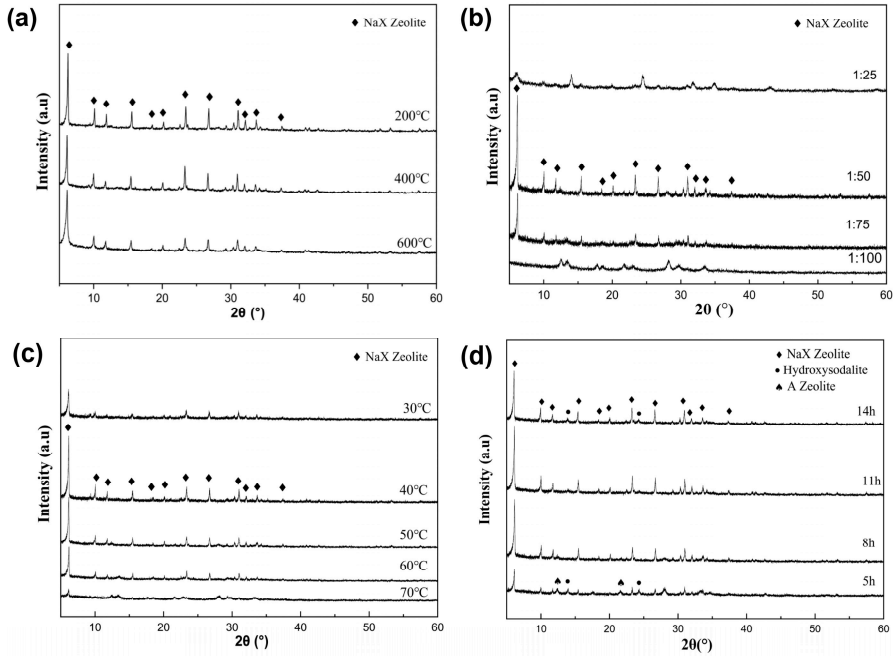

Figure 4. (**a**) XRD patterns of the products synthesized at different alkali fusion treatment temperatures. (**b**) XRD patterns of the products synthesized at different H_2O/Na_2O ratios. (**c**) XRD patterns of the products synthesized at different hydrothermal temperatures. (**d**) XRD patterns of products synthesized at different hydrothermal times.

Aging is the time between the formation of aluminosilicate gels and their crystallization. This process plays a very important role in the nucleation of amorphous gels. During the aging process, the composition and structure of the gel undergo changes, which is a slow nucleation process. During the middle and later stages of aging, seed nuclei remain in a dormant state, and upon being heated to the crystallization temperature, these nuclei gradually undergo growth to form zeolite products. Appropriate aging can increase the nucleation rate, shorten the induction period and crystallization duration, reduce crystal size, and increase the number of crystals. In this experiment, the effects of different aging temperatures on the obtained zeolite products were investigated under the conditions of a crystallization temperature of 90 °C, crystallization time of 8 h, and H_2O/Na_2O ratio of 50. The results as shown in Figure 4c indicate that the crystallinity of zeolite decreased with an increase in aging temperature, with a very low yield of NaX zeolite observed at an aging temperature of 70 °C. In contrast, NaX zeolite with high crystallinity and a nearly pure phase was obtained at an aging temperature of 40 °C, indicating that lower temperatures are favorable for the formation of zeolite nuclei during aging.

To investigate the effect of different crystallization times on the zeolite products, the aged stock solution was crystallized at 90 °C for 5 h, 8 h, 11 h, and 14 h. The XRD pattern in Figure 4d indicates that the crystallinity of NaX zeolite initially increases and then decreases as the crystallization time is prolonged. After 5 h of crystallization, NaX zeolite was obtained, but with a minor formation of zeolite A and hydroxysodalite. After 8 h of crystallization, an almost pure phase of NaX zeolite was successfully synthesized. Extending the crystallization time to 11 h resulted in further crystal growth and perfection, and the characteristic diffraction peaks continued to increase. However, the characteristic diffraction peaks of hydroxysodalite also began to emerge at this stage. The 14 h crys-

tallization resulted in a decrease in the intensity of the NaX diffraction peak and a more pronounced characteristic peak of hydroxysodalite. Excessive crystallization time may lead to the disintegration of some NaX zeolite crystals and partial conversion to zeolites A. Therefore, the optimal crystallization time for zeolite synthesized through this method is approximately 8 h.

3.3. Adsorption Performance of Zeolite NaX

In the adsorption experiments, the influences of adsorption time, initial concentration of Pb^{2+}, NaX molecular sieve dosage, and pH value on the removal rate of Pb^{2+} were investigated. As shown in Figure 5a, with the increase in adsorption time, the removal rate of Pb^{2+} rose rapidly in the first 60 min and approached approximately 90%. As the adsorption time was prolonged further, the removal rate increased gradually to around 95%. At the initial stage of adsorption, Pb^{2+} rapidly occupied the active sites on the surface of the molecular sieve, leading to a rapid escalation in the removal rate. After 60 min of adsorption, the active sites of the molecular sieve were gradually occupied by Pb^{2+}, and the removal rate increased at a slower pace until the adsorption reached equilibrium. Figure 5b illustrates the influence of different initial concentrations of Pb^{2+} in the simulated wastewater on the removal rate. In general, the initial concentration has little influence on the effectiveness of clay-based zeolite molecular sieves in removing Pb^{2+}. The removal effect can be stabilized at approximately 95%. Nevertheless, at the lower Pb^{2+} concentration range of 0~40 mg/L, the removal rate is relatively low and shows a slowly increasing trend. The possible reason for this phenomenon is that at low initial concentrations, it is mainly influenced by adsorption kinetics. Although there are abundant active sites on the surface of the molecular sieve, the low concentration of Pb^{2+} leads to a low removal rate due to the reduced chance of mutual contact and collision between the molecular sieve and Pb^{2+}. Figure 5c illustrates the effect of different zeolite dosages on the removal of Pb^{2+}. The adsorption results indicated that the removal rate of Pb^{2+} increased with the increase in molecular sieve dosage. Particularly, when the molecular sieve dosage was in the range of 0.2~1.0 g/L, the removal rate increased rapidly. This might be attributed to the fact that increasing the amount of molecular sieves provides more adsorption sites, thereby promoting adsorption. At a molecular sieve dosage of 0.9 g/L, the removal rate of Pb^{2+} by NaX zeolite was 93.13%. As the dosage of the molecular sieve continued to increase, the removal rate eventually reached more than 96%, but the growth was slow. This is because most of the heavy metal ions had already been adsorbed and the adsorption had reached equilibrium. Considering economic factors, a molecular sieve dosage of 0.9 g/L was selected as the optimal dosage for the experiment. Figure 5d depicts the effect of solution pH on the efficacy of 13X zeolite in removing Pb^{2+}. The results suggest that the initial pH of the simulated wastewater is a crucial influencing factor in the adsorption process. As can be seen, NaX zeolite has a lower adsorption capacity at pH = 1~3. This is because there is adsorption competition between H^+ and Pb^{2+} in the solution under strong acidic conditions. As a result, H^+ is preferentially exchanged with Na^+ on the surface of NaX zeolites, negatively affecting the adsorption of Pb^{2+}. The removal rate of NaX zeolite for Pb^{2+} gradually increases with the increase in pH. Overall, the clay-based NaX zeolite exhibits good adsorption capacity under weakly acidic, neutral, and alkaline wastewater conditions, demonstrating good adaptability. However, when the solution is alkaline, especially when the pH is greater than 7, Pb^{2+} and OH^- produce precipitation. Although the removal rate does not decrease, the adsorption effect is weakened and the metal precipitation effect is enhanced. Therefore, pH = 5 was selected as the optimal initial pH value in the experiment.

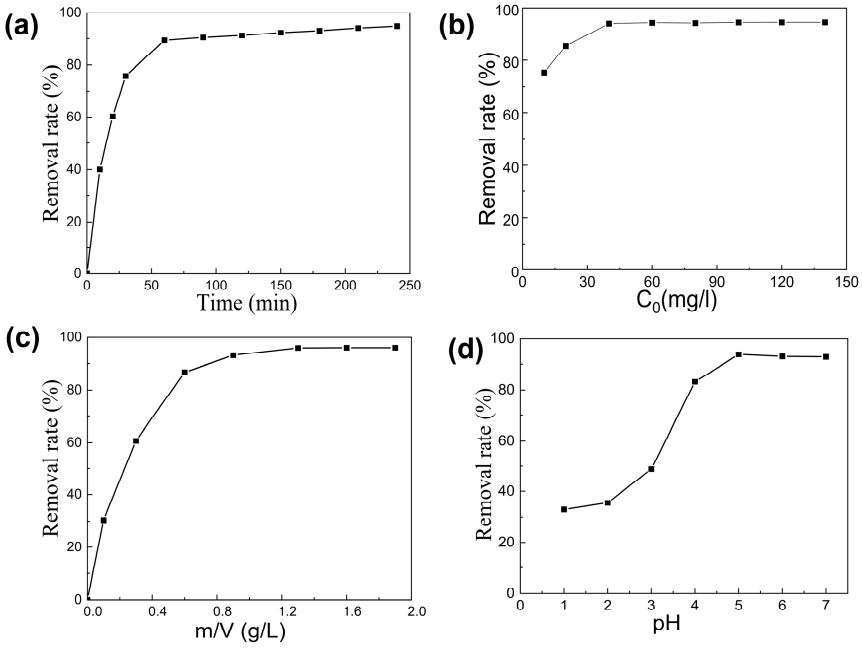

Figure 5. Variation curves of Pb^{2+} removal rate by clay-based NaX zeolite with (**a**) adsorption time, (**b**) initial Pb^{2+} concentration, (**c**) molecular sieve dosage, (**d**) pH value of wastewater solution.

3.4. Adsorption Isotherm and Adsorption Kinetic Analysis

The process of clay-based NaX zeolite adsorbing Pb^{2+} in solution at 25 °C can be studied by using the Langmuir equation and Freundlich equation that describe the solid–liquid isothermal adsorption process.

Langmuir isothermal equation:

$$Q_e = \frac{K_L C_e Q_{max}}{1 + K_L C_e} \tag{3}$$

Freundlich isothermal equation:

$$Q_e = K_F C_e^{1/n} \tag{4}$$

Q_e is the equilibrium adsorption capacity (g/mg); K_L is the Langmuir equilibrium adsorption constant (L/mg); C_e is the molar concentration (mg/L) of Pb^{2+} in the solution at equilibrium; Q_{max} is the saturated adsorption capacity (mg/g); K_F is the Freundlich constant (mg/g) $(mg/L)^{-n}$); and n is the Freundlich constant.

The adsorption mechanism is explored by using adsorption kinetic laws. The pseudo-first-order Equation (5) and pseudo-second-order Equation (6) models are used to further analyze the adsorption process.

$$\ln(Q_e - Q_t) = \ln Q_e k_1 t \tag{5}$$

$$t/Q_t = \frac{1}{k_2 Q_e^2} + t/Q_e \tag{6}$$

Q_e (mg/g) is the equilibrium adsorption capacity of Pb^{2+}, Q_t (mg/g) is the adsorption capacity of Pb^{2+} at time t, k_1 (min^{-1}) is the pseudo-first-order rate constant, t (min) is the time, and k_2 [g/(mg min)] is the pseudo-second-order rate constant.

The fitting results of the Langmuir and Freundlich models for the adsorption of Pb^{2+} by clay-based NaX zeolite are shown in Figure 6 and Table 2. It can be seen that, compared with the Freundlich model, the Langmuir adsorption isotherm equation can better describe the adsorption law of attapulgite-type 13X zeolite on Pb^{2+}. The adsorption process is

monolayer adsorption. The Q_{max} is about 114.58 g/mg, and the saturated adsorption capacity measured experimentally is 113.28 g/mg.

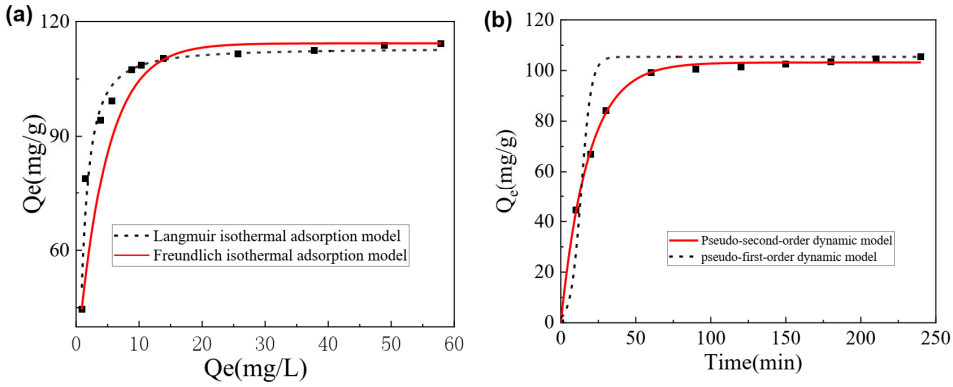

Figure 6. Pseudo-first-order and pseudo-second-order dynamic models for Pb^{2+} adsorption by NaX zeolite (**a**), Langmuir and Freundlich isothermal model for Pb^{2+} adsorption by NaX zeolite (**b**).

Table 2. Parameters of Langmuir and Freundlich adsorption isotherm equations for the adsorption of Pb^{2+} by clay-based NaX zeolite.

Langmuir Constants			**Freundlich Constants**		
Q_{max}	K_L	R^2	Q_{max}	K_F	R^2
114.58	5.3	0.922	117.32	24.15	0.756

The adsorption curves after kinetic simulation are shown in Figure 6b and Table 3. It can be seen that although the saturated adsorption capacity (102.695 mg/g) fitted by the pseudo-first-order kinetic model is close to the equilibrium adsorption capacity (102.21 mg/g) measured experimentally, the fitting curve has R^2 (0.875) with a relatively large deviation. It can be inferred that this process does not fully conform to the adsorption process of Pb^{2+} by NaX zeolite. Judging from the kinetic second-order fitting curve, it is highly consistent with the experimental data with R^2 (0.998). Therefore, the adsorption process of Pb^{2+} by clay-based NaX zeolite is more in line with the pseudo-second-order kinetic model. The maximum adsorption capacity of this zeolite is about 98.8 g/mg, which is higher than the maximum adsorption capacity reported in the literature in Table 4. It has great application value in the field of heavy metal adsorption.

Table 3. Results of pseudo-first-order and second-order kinetic models for the adsorption of Pb^{2+} by clay-based NaX zeolite.

Pseudo-First-Order			**Pseudo-Second-Order Kinetic**		
Q_e	K_1	R^2	Q_e	K_2	R^2
102.695	14.36	0.875	98.814	0.038	0.998

Table 4. Comparison with the maximum adsorption of Pb^{2+} by zeolite adsorbents reported in the available literature.

Absorbent	**pH**	Q_{max} **mg/g**	**Isotherm Model**	**Reference**
Zeolite composites	6	47.619	Langmuir	[36]
Y Zeolite	4.7	57.47	Langmuir	[37]
5A Zeolite	5.5	46.67	Langmuir	[38]
Sodium aluminum silicate hydrate/ANA	5.5	58.86	Langmuir	[39]
Natural zeolite	7	7.59	Langmuir	[40]
Zeolite + tuff	3.5	27.548	Langmuir	[41]

4. Conclusions

In this study, zeolite NaX was successfully synthesized using activated low-quality mixed-dimensional attapulgite clay. This synthesis process was not only simple but also highly efficient, offering a promising direction for the utilization of low-grade natural clay mineral resources. In addition, the optimum synthesis conditions were obtained as follows: an alkali melting temperature of 200 °C, a water-to-sodium ratio of 50:1, an aging temperature of 40 °C, and a crystallization time of 11 h at 90 °C. The prepared zeolite was well crystallized with a regular octahedral structure, a specific surface area of 328.43 m^2/g, and a microporous volume of 0.23 cm^3/g. The results of the Pb^{2+} adsorption experiments indicated that the clay-based NaX molecular sieve has a strong removal ability for Pb^{2+} in the simulated wastewater. Under the conditions of 25 °C, pH = 5, an adsorbent dosage of 0.9 g/L, and an adsorption time of 60 min, the removal rate of Pb^{2+} with an initial concentration ranging from 40 to 140 mg/L can reach more than 95%, which represents a good adsorption effect. This low-grade mixed-dimensional attapulgite clay proved to be an ideal raw material for the synthesis of NaX zeolite, showcasing immense industrial application value.

Author Contributions: Conceptualization, K.Z. and Y.T.; methodology, K.Z., Y.T. and M.F.; software, M.F.; validation, M.F., Z.S., K.Z. and Y.T.; formal analysis, Z.S.; investigation, M.F. and Z.S.; resources, K.Z. and Y.T.; data curation, M.F. and Z.S.; writing—original draft preparation, M.F. and K.Z.; writing—review and editing, M.F.; visualization, M.F.; supervision, K.Z. and Y.T.; project administration, K.Z. and Y.T.; funding acquisition, Y.T. All authors have read and agreed to the published version of the manuscript.

Funding: This work was funded by the Key Laboratory of Hexi Corridor Resources Utilization (XZ2303), the Higher Education Innovation Fund Project of Gansu (2022B-184), 2022 Undergraduate Innovation and Entrepreneurship Training Program Project (S202210740100), National Natural Science Foundation Regional Fund (22362015). The Doctoral Research Initiation Fund Project of Hexi University (KYQD2020033).

Data Availability Statement: The data presented in this study are available in the article.

Acknowledgments: The authors thank the Key Laboratory of Hexi Corridor Resources Utilization for providing detection methods such as XRD, SEM, FT-IR, and BET.

Conflicts of Interest: The authors declare no conflicts of interest.

References

1. Chen, M.Y.; Nong, S.Y.; Zhao, Y.T.; Riaz, M.S.; Xiao, Y.; Molokeev, M.S.; Huang, F.Q. Renewable P-type zeolite for superior absorption of heavy metals: Isotherms, kinetics, and mechanism. *Sci. Total Environ.* **2020**, *726*, 138535–138540. [CrossRef] [PubMed]
2. Qasem, N.A.A.; Mohammed, R.H.; Lawal, D.U. Removal of heavy metal ions from wastewater: A comprehensive and critical review. *npj Clean Water* **2021**, *4*, 36–42. [CrossRef]
3. Wei, E.; Wang, K.; Muhammad, Y.; Chen, S.; Dong, D.; Wei, Y.Z.; Fujita, T. Preparation and conversion mechanism of different geopolymer-based zeolite microspheres and their adsorption properties for Pb^{2+}. *Sep. Purif. Technol.* **2022**, *282*, 119971–119980. [CrossRef]
4. Azizi, D.; Ibsaine, F.; Dionne, J.; Pasquier, L.C.; Coudert, L.; Blais, J.F. Microporous and macroporous materials state-of-the-art of the technologies in zeolitization of aluminosilicate bearing residues from mining and metallurgical industries: A comprehensive review. *Micropor. Mesopor. Mater.* **2021**, *318*, 111029–111045. [CrossRef]
5. Tran-Nguyen, P.L.; Ly, K.-P.; Thanh, L.H.V.; Angkawijaya, A.E.; Santoso, S.P.; Tran, N.P.D.; Tsai, M.L.; Ju, Y.H. Facile synthesis of zeolite NaX using rice husk ash without pretreatment. *J. Taiwan Inst. Chem. E* **2021**, *123*, 338–345. [CrossRef]
6. Wang, L.; Liu, J.; Lin, C.; Shang, H.; Yang, J.; Li, L.; Li, J. Effects of different alkali metal cations in FAU zeolites on the separation performance of CO_2/N_2O. Chem. *Eng. J.* **2022**, *431*, 134257–134266. [CrossRef]
7. Mokrzycki, J.; Fedyna, M.; Marzec, M.; Panek, R.; Szerement, J.; Marcińska-Mazur, L.; Jarosz, R.; Bajda, T.; Franus, W.; Mierzwa-Hersztek, M. The influence of zeolite X ion-exchangeable forms and impregnation with copper nitrate on the adsorption of phosphate ions from aqueous solutions. *J. Water Process. Eng.* **2022**, *50*, 103299–103308. [CrossRef]
8. Han, L.; Wang, X.; Wu, B.; Zhu, S.; Wang, J.; Zhang, Y. In-situ synthesis of zeolite X in foam geopolymer as a CO_2 adsorbent. *J. Clean. Prod.* **2022**, *372*, 133591–133598. [CrossRef]

9. Li, X.; Han, H.; Xu, W.; Hwang, S.J.; Shi, Z.; Lu, P.; Bhan, A.; Tsapatsis, M. Acid catalysis over low-silica faujasite zeolites. *J. Am. Chem. Soc.* **2022**, *144*, 9324–9329. [CrossRef]
10. Hartanto, D.; Kurniawati, R.; Pambudi, A.B.; Utomo, W.P.; Loon, W.; Nur, H. One-pot non-template synthesis of hierarchical ZSM-5 from kaolin source. *Solid State Sci.* **2019**, *87*, 150–154. [CrossRef]
11. Ma, Y.; Yan, C.; Alshameri, A.; Qiu, X.; Zhou, C.; Li, D. Synthesis and characterization of 13X zeolite from low-grade natural kaolin. *Adv. Powder Technol.* **2014**, *25*, 495–499. [CrossRef]
12. Yue, Y.Y.; Gao, X.X.; Liu, T.; Liu, H.Y.; Wang, T.H.; Yuan, P.; Zhu, H.B.; Bai, Z.S.; Bao, X.J. Template free synthesis of hierarchical porous zeolite Beta with natural kaolin clay as alumina source. *Micropor. Mesopor. Mater.* **2020**, *293*, 109772–109811. [CrossRef]
13. Tang, L.J.; Xie, X.Z.; Huang, Y.X.; Pan, Y.M.; Mi, J.X. Phase diagram for hydrothermal alkali activation of kaolin and quartz: Optimal digestion for the synthesis of zeolites. *Mater. Chem. Phys.* **2022**, *290*, 126570–126580. [CrossRef]
14. Chen, S.; Guan, D.D.; Zhang, Y.; Wang, Z.; Jiang, N.Z. Composition and kinetic study on template- and solvent-free synthesis of ZSM-5 using leached illite clay. *Micropor. Mesopor. Mater.* **2019**, *285*, 170–177. [CrossRef]
15. Han, S.Y.; Liu, Y.; Yin, C.R.; Jiang, N.Z. Fast synthesis of submicron ZSM-zeolite from leached illite clay using a seed-assisted method. *Micropor. Mesopor. Mater.* **2019**, *275*, 223–228. [CrossRef]
16. Liu, Y.; Han, S.Y.; Guan, D.D.; Chen, S.; Wu, Y.H.; Yang, Y.; Jiang, N.Z. Rapid green synthesis of ZSM-5 zeolite from leached illite clay. *Micropor. Mesopor. Mater.* **2019**, *280*, 324–330. [CrossRef]
17. Li, X.; Han, S.; Guan, D.; Jiang, N.; Park, S.E. Rapid direct synthesis of nano-H-ZSM-5 from leached illite via solid-like-state conversion-based crystallization. *Appl. Clay Sci.* **2021**, *203*, 106028–106039. [CrossRef]
18. Chen, C.; Park, D.W.; Ahn, W.S. CO_2 capture using zeolite 13X prepared from bentonite. *Appl. Surf. Sci.* **2014**, *292*, 63–67. [CrossRef]
19. Hosseini, M.S.H.; Eslami, F.; Karimzadeh, R. Organic contaminants removal from industrial wastewater by CTAB treated synthetic zeolite Y. *J. Environ. Manag.* **2019**, *233*, 785–792. [CrossRef]
20. Hamidi, R.; Khoshbin, R.; Karimzadeh, R. A new approach for synthesis of well-crystallized Y zeolite from bentonite and rice husk ash used in Ni-Mo/Al_2O_3-Y hybrid nanocatalyst for hydrocracking of heavy oil. *Adv. Powder Technol.* **2021**, *32*, 524–534. [CrossRef]
21. Yao, G.Y.; Lei, J.J.; Zhang, X.Y.; Sun, Z.M.; Zheng, S.L. One-step hydrothermal synthesis of zeolite X powder from natural low-grade diatomite. *Materials* **2018**, *11*, 906. [CrossRef]
22. Moreno-Maroto, J.M.; Alonso-Azcárate, J.; Martínez-García, C.; Romero, M.; López-Delgado, A.; Cotes-Palomino, T. Zeolitization of diatomite residues by a simple method. *Appl. Sci.* **2022**, *12*, 10977. [CrossRef]
23. Sun, L.M.; Wu, J.S.; Wang, J.S.; Yu, G.; Liu, J.C.; Du, Y.C.; Li, Y.L.; Li, H.Y. Controlled synthesis of zeolite adsorbent from low-grade diatomite: A case study of self-assembled sodalite microspheres. *J. Environ. Sci.* **2020**, *91*, 92–104. [CrossRef]
24. Stafin, G.; Grzebielucka, E.C.; Antunes, S.R.M.; Borges, C.P.F.; Souza, D.C.F.D. Synthesis of zeolites from residual diatomite using a microwave-assisted hydrothermal method. *Waste Manag.* **2021**, *126*, 853–860. [CrossRef]
25. Zhu, T.; Zhang, X.; Han, Y.; Liu, T.; Wang, B.; Zhang, Z. Preparation of zeolite X by the aluminum residue from coal fly ash for the adsorption of volatile organic compounds. *Front. Chem.* **2019**, *7*, 341–349. [CrossRef]
26. Makgabutlane, B.; Nthunya, L.N.; Nxumalo, E.N.; Musyoka, N.M.; Mhlanga, S.D. Microwave irradiation-assisted synthesis of zeolites from coal fly ash: An optimization study for a sustainable and efficient production process. *ACS Omega* **2020**, *5*, 25000–25008. [CrossRef]
27. Boycheva, S.; Zgureva, D.; Lazarova, H.; Popova, M. Comparative studies of carbon capture onto coal fly ash zeolites Na-X and Na-Ca-X. *Chemosphere* **2021**, *271*, 129505–129514. [CrossRef]
28. Wu, Y.; Liang, G.; Zhao, X.; Wang, H.; Qu, Z. Flexible textural design of ZSM-5 zeolite adsorbent from coal fly ash via solvent-free method for toluene elimination. *J. Environ. Chem.* **2023**, *11*, 109589. [CrossRef]
29. Li, X.Y.; Jiang, Y.; Liu, X.Q.; Shi, L.Y.; Zhang, D.Y.; Sun, L.B. Direct synthesis of zeolites from a natural clay, attapulgite. *ACS Sustain. Chem. Eng.* **2017**, *5*, 6124–6130. [CrossRef]
30. Wu, M.; Jiang, W.B.; Jiang, J.L.; Zou, Y.Q.; Shi, Y.Y. Synthesis of ZSM-5 zeolites using palygorskite as raw material under solvent-free conditions. *Bull. Mater. Sci.* **2020**, *43*, 289–298. [CrossRef]
31. Li, H.; Zhang, Y.; Diao, J.; Qiang, M.; Chen, Z. Synthesis and photocatalytic activity of hierarchical Zn-ZSM-5 structures. *Catalysts* **2021**, *11*, 797. [CrossRef]
32. Xie, Q.Q.; Chen, T.H.; Zhou, H.; Xu, X.C.; Xu, H.F.; Ji, J.F.; Lu, H.Y.; Balsam, W. Mechanism of palygorskite formation in the Red Clay Formation on the Chinese Loess Plateau, northwest China. *Geoderma* **2013**, *192*, 39–49. [CrossRef]
33. Zhang, S.; Liu, L.; Liu, Q.; Zhang, B.; Qiao, Z.; Teppen, B.J. Genesis of palygorskite in the neogene baiyanghe formation in Yangtaiwatan basin, northwest China, based on the mineralogical characteristics and occurrence of enriched trace elements and ree. *Clays Clay Miner.* **2021**, *69*, 23–27. [CrossRef]
34. Lu, Y.; Wang, A. From structure evolution of palygorskite to functional material: A review. *Micropor. Mesopor. Mater.* **2022**, *333*, 111765–111783. [CrossRef]
35. He, Y.; Tang, S.; Yin, S.; Li, S. Research progress on green synthesis of various high-purity zeolites from natural material-kaolin. *J. Clean. Prod.* **2021**, *306*, 127248–127266. [CrossRef]
36. Isawi, H. Using Zeolite/Polyvinyl alcohol/sodium alginate nanocomposite beads for removal of some heavy metals from wastewater. *Arab. J. Chem.* **2020**, *13*, 5691–5716. [CrossRef]

37. Hamoudi, S.A.; Khelifa, N.; Loubna, N.; Hemidouche, S.; Boudjemaa, A.; Boucheffa, Y. Removal of Pb^{2+} and Cd^{2+} by adsorption onto Y zeolite and its selectivity of retention in an actual contaminated effluent. *Colloid Polym. Sci.* **2023**, *301*, 631–645. [CrossRef]
38. Mayta-Armas, A.F.; Yamerson, C.H.; Jemina, P.; Yéssica, B.; Noemi-Raquel, C.; Juan, A. Enhanced removal of As(V) and Pb(II) from drinking and irrigating water effluents using hydrothermally synthesized zeolite 5A. *Water* **2023**, *15*, 1892. [CrossRef]
39. Abdelrahman, E.A.; Ahmed; Subaihi, A.; Ahmed, M.; Mohammed, A.A.; Faisal, K.A.; Hany, M.Y. Facile fabrication of novel analcime/sodium aluminum silicate hydrate and zeolite Y/faujasite mesoporous nanocomposites for efficient removal of Cu(II) and Pb(II) ions from aqueous media. *J. Mater. Res. Technol.* **2020**, *9*, 7900–7914. [CrossRef]
40. Wangi, G.M.; Olupot, P.W.; Byaruhanga, J.; Kulabako, R. Characterization of natural zeolite and determination of its ion-exchange potential for selected metal ions in water. *Environ. Process.* **2023**, *10*, 53. [CrossRef]
41. Zendelska, A.; Golomeova, M.; Golomeov, B.; Krstev, B. Removal of zinc ions from acid aqueous solutions and acid mine drainage using zeolite-bearing tuff. *Mine Water Environ.* **2019**, *38*, 187–196. [CrossRef]